

CASC-AI: Consensus-aware Self-corrective AI Agents for Noise Cell Segmentation

Ruining Deng ^{1,2}	R.DENG@VANDERBILT.EDU
Yihe Yang ¹	YIY4007@MED.CORNELL.EDU
David J. Pisapia ¹	DJP2002@MED.CORNELL.EDU
Benjamin Liechty ¹	BEL9057@MED.CORNELL.EDU
Junchao Zhu ²	JUNCHAO.ZHU@VANDERBILT.EDU
Juming Xiong ²	JUMING.XIONG@VANDERBILT.EDU
Junlin Guo ²	JUNLIN.GUO@VANDERBILT.EDU
Zhengyi Lu ²	ZHENGYI.LU@VANDERBILT.EDU
Jiacheng Wang ²	JIACHENG.WANG.1@VANDERBILT.EDU
Xing Yao ²	XING.YAO@VANDERBILT.EDU
Runxuan Yu ²	RUNXUAN.YU@VANDERBILT.EDU
Rendong Zhang ²	RENDONG.ZHANG@VANDERBILT.EDU
Gaurav Rudravaram ²	GAURAV.RUDRAVARAM@VANDERBILT.EDU
Mengmeng Yin ³	MENGMENG.YIN.1@VUMC.ORG
Pinaki Sarder ⁴	PINAKI.SARDER@UFL.EDU
Haichun Yang ³	HAICHUN.YANG@VUMC.ORG
Yuankai Huo ^{2,3}	YUANKAI.HUO@VANDERBILT.EDU
Mert R. Sabuncu ^{1,5}	MSABUNCU@CORNELL.EDU

¹ Weill Cornell Medicine, New York, NY 10021

² Vanderbilt University, Nashville, TN, USA 37215

³ Vanderbilt University Medical Center, Nashville, TN, USA 37232

⁴ University of Florida, Gainesville, FL, USA 32611

⁵ Cornell Tech, New York, NY, USA 10044

Editors: Under Review for MIDL 2025

Abstract

Multi-class cell segmentation in high-resolution gigapixel whole slide images (WSI) is crucial for various clinical applications. However, training such models typically requires labor-intensive, pixel-wise annotations by domain experts. Recent efforts have democratized this process by involving lay annotators without medical expertise. However, conventional non-agent-based approaches struggle to handle annotation noise adaptively, as they lack mechanisms to mitigate false positives (FP) and false negatives (FN) at both the image-feature and pixel levels. In this paper, we propose a consensus-aware self-corrective AI agent that leverages the Consensus Matrix to guide its learning process. The Consensus Matrix defines regions where both the AI and annotators agree on cell and non-cell annotations, which are prioritized with stronger supervision. Conversely, areas of disagreement are adaptively weighted based on their feature similarity to high-confidence agreement regions, with more similar regions receiving greater attention. Additionally, contrastive learning is employed to separate features of noisy regions from those of reliable agreement regions by maximizing their dissimilarity. This paradigm enables the AI to iteratively refine noisy labels, enhancing its robustness. Validated on one real-world lay-annotated cell dataset and two simulated noisy datasets, our method demonstrates improved segmentation performance, effectively correcting FP and FN errors and showcasing its potential for training

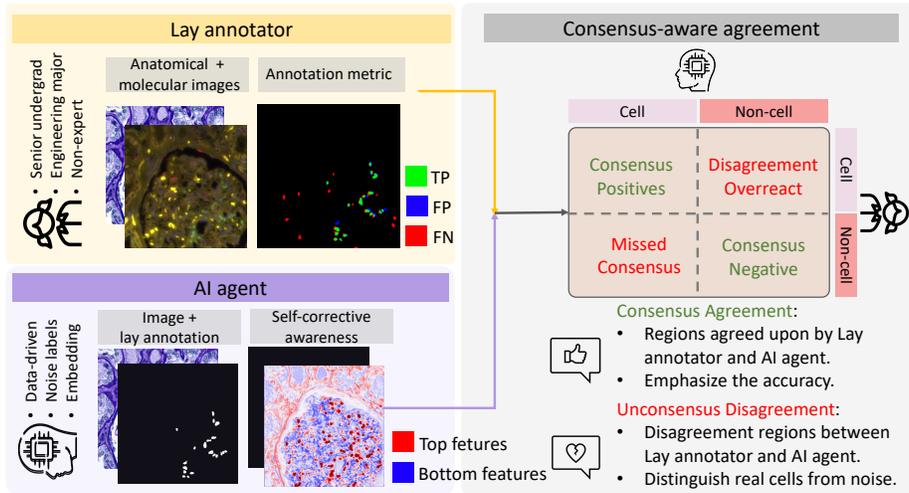


Figure 1: **Consensus-awareness self-corrective AI agent.** We propose a Consensus-Aware Self-Corrective AI Agent for robust cell segmentation with noisy training data. The AI leverages the CM to guide learning, prioritizing CP and CN regions with stronger supervision, while adaptively weighting DO and MC regions based on their similarity to reliable CP regions. Additionally, contrastive learning is employed to separate noisy and reliable features, iteratively refining labels. This approach improves segmentation by leveraging pixel- and feature-level agreement with lay annotators.

robust models on noisy datasets. The official implementation and cell annotations are publicly available at <https://github.com/ddrrnn123/CASC-AI>.

Keywords: Consensus matrix, Corrective Learning, Noisy label learning, Cell Segmentation

1. Introduction

Multi-class cell segmentation is essential for analyzing tissue samples in digital pathology, often serving as the initial step in extracting biological signals crucial for accurate disease diagnosis and treatment planning (Caicedo et al., 2017; Deng et al., 2020; Keren et al., 2018; Pratapa et al., 2021; Litjens et al., 2017; Border et al., 2024). Accurate cell quantification aids pathologists in diagnosing diseases (Comaniciu and Meer, 2002; Xing and Yang, 2016), determining disease progression (Olindo et al., 2005), assessing severity (Wijeratne et al., 2018), and evaluating treatment efficacy (Jiménez-Heffernan et al., 2006). For instance, the distribution and density of cells in the glomerulus (e.g., podocytes, mesangial cells, endothelial cells, and epithelial cells) can serve as indicators of functional injury in renal pathology (Imig et al., 2022). However, cell-level characterization is challenging even for experienced pathologists due to the long annotation time, extensive labor required, significant variability in cell morphology (Zheng et al., 2021), and the potential for human error. Needless to mention the rigorous medical training required for a pathologist. Training automatic deep learning models for cell segmentation can significantly reduce the workload of manual cell quantification (Greenwald et al., 2022; Pratapa et al., 2021; Lucarelli et al., 2024; Guo et al., 2024). These models require large-scale data collection to achieve satisfactory segmentation performance.

Previous efforts have democratized the annotation process by involving lay annotators without medical expertise and integrating pair-wise molecular images with pathological

images, resulting in a substantial number of accurate cell annotations for training AI models (Deng et al., 2023). However, this approach inevitably introduces noise and errors, necessitating correction by experienced pathologists. Directly training models on such noisy labels often leads to suboptimal performance. This highlights the urgent need for a corrective learning paradigm that effectively addresses label noise during cell segmentation model training (Vădineanu et al., 2022; Karimi et al., 2020). Previous research on noisy-label learning has focused on defining efficient loss functions (Zhang and Sabuncu, 2018; Wang et al., 2020; Ma et al., 2020) and leveraging multi-network strategies (Zhang et al., 2020; Han et al., 2018; Lu et al., 2023; Guo et al., 2023). However, these approaches largely overlook the integration of feature-level analysis with pixel-level analysis to effectively identify annotation errors at the pixel level.

In this work, we propose a Consensus-Aware Self-Corrective AI Agent (CASC-AI) that incorporates insights from the Consensus Matrix (CM) to guide its learning process (as shown in Fig. 1). Unlike conventional heuristic-based correction methods, CASC-AI actively learns from noisy annotations, leveraging both pixel-wise and feature-wise information to refine its predictions iteratively. The AI agent autonomously detects patterns in annotation errors and adapts its training accordingly, unlike non-AI approaches that rely on predefined rules or manual intervention. Additionally, the AI agent utilizes contrastive learning to distinguish noisy labels from high-confidence regions by maximizing feature dissimilarity, which improves its robustness against annotation errors. This enables progressive self-correction, where the model continuously refines its understanding of cell features without explicit human intervention. The contributions of this paper is threefold:

- A Consensus-Aware Self-Corrective AI Agent is designed to provide robust cell segmentation when training data contains noise.
- A noise-generation process is introduced for pathological cell images to simulate realistic noise for label analysis.
- By integrating Consensus Matrix insights at both the pixel and feature levels, the proposed method demonstrates improved segmentation performance, effectively addressing FP and FN errors, showcasing its potential for training robust models on noisy datasets.

2. Method

Introducing lay annotators into the labeling process significantly increases the volume of annotations available for training deep learning models. However, it also introduces noise and errors due to human visual limitations and variability among annotators. With the rapid development of deep learning, AI has demonstrated its capability in representing images (Oquab et al., 2023; Huang et al., 2021), providing reliable and stable latent features for image understanding. Therefore, the proposed CASC-AI aims to combine the strengths of human expertise and AI capability during the training phase, guiding the model to capture accurate information from lay annotations while distinguishing potential noise at the pixel level. The overall learning paradigm consists of three components: (1) Consensus Matrix, (2) Agreement-Guided Supervision, and (3) Contrastive Noise Separation.

2.1. Consensus Matrix

To capture the agreement between lay annotators and the AI agent, we define a Consensus Matrix (in Fig. 1), inspired by the confusion matrix, to guide pixel-level image understanding. The matrix is composed of the following components:

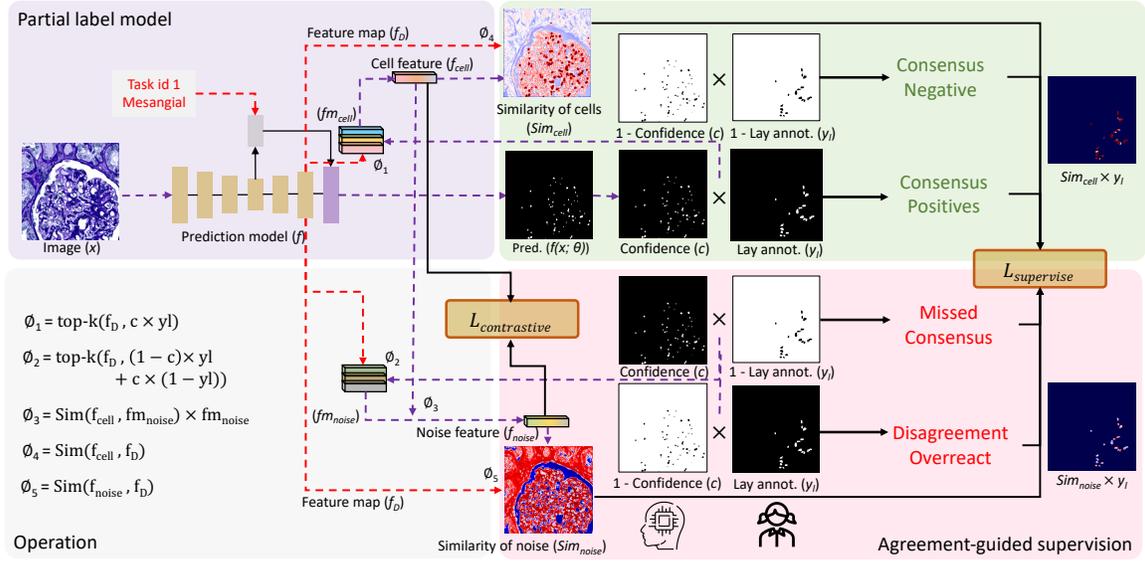


Figure 2: **Overview of the Consensus-Aware Agreement-Guided Supervision Framework.** The architecture integrates AI-derived confidence maps (c) and lay annotations (y_l) to identify consensus-positive (CP), consensus-negative (CN), and disagreement regions (DO, MC). Key steps include the derivation of cell features (f_{cell}) and noise features (f_{noise}), the computation of similarity scores (sim_{cell} , sim_{noise}), and their application in contrastive noise separation and supervised learning loss ($\mathcal{L}_{supervise}$, $\mathcal{L}_{contrastive}$). This framework emphasizes robust training by focusing on regions of agreement and leveraging disagreement as informative cues for improved cell segmentation accuracy.

Consensus Positives (CP): Regions where both the AI and annotators agree on a “cell” annotation. These regions represent strong consensus for action, where both parties confidently identify cells.

Consensus Negatives (CN): Regions where both the AI and annotators agree on a “non-cell” annotation. These regions reflect mutual agreement to abstain from action, ensuring non-cell regions are left unannotated.

Disagreement Overreach (DO): Regions where the AI identifies a “cell,” but annotators label it as “non-cell.” These regions highlight overconfidence or misclassification by the AI, leading to unnecessary action.

Missed Consensus (MC): Regions where the AI labels a region as “non-cell,” but annotators identify it as a “cell.” These regions represent missed opportunities to take action due to a lack of agreement on true cell regions.

2.2. Consensus-aware Agreement-Guided Supervision

Building on our previous works (Deng et al., 2023, 2024a), we select a token-based residual U-Net from (Deng et al., 2024b) as the backbone for cell segmentation tasks. This backbone demonstrates superior performance in multi-class cell segmentation using partially labeled datasets. As illustrated in Fig. 2, the model outputs the final prediction logits $p \in \mathbb{R}^{2 \times W \times H}$, the pixel-level feature map of the decoder’s last layer $f_D \in \mathbb{R}^{C_h \times W \times H}$, and a confidence map $c \in \mathbb{R}^{1 \times W \times H}$, defined as:

$$c = \text{softmax}(p)[1, \dots] \quad (1)$$

Where W and H are the width and height of the input image, while Ch represents the number of channels in the decoder’s last layer. The confidence map $c \in (0, 1)$ indicates the confidence level of predictions: values closer to 1 suggest stronger confidence in identifying a region as a cell, while values closer to 0 suggest a higher likelihood of non-cell regions.

2.2.1. CONSENSUS CELL FEATURE DISTILLATION

Using the confidence map c from the AI agent, we combine it with lay annotations y_l to identify pixel locations with the highest agreement scores a_{CP} in CP regions. These regions are used to distill features f_{cell} that best represent cell types. The computation for a_{CP} and f_{cell} is defined in Eq. 5 in the Appendix A (annotated as ϕ_1 in Fig. 2).

2.2.2. UNCONSENSUS NOISE FEATURE DISTILLATION

In DO and MC regions, where the AI agent and lay annotators disagree, we identify top pixel locations with the highest disagreement scores a_{DO} and a_{MC} . Features from these regions $f_{m_{\text{noise}}}$ potentially contain both real cells and noise, as represented in Eq. 6 in the Appendix A (annotated as ϕ_2 in Fig. 2).

When aggregating potential noise features $f_{m_{\text{noise}}}$ into the distilled noise feature f_{noise} , we calculate the similarity s_{cell} between the potential noise features $f_{m_{\text{noise}}}$ and the cell feature f_{cell} . Using a weighted sum, we derive the final noise feature f_{noise} , based on the assumption that noise features in these regions are dissimilar to cell features. The process is defined in Eq. 7 in Appendix A (highlighted as ϕ_3 in Fig. 2).

We compute the similarity between the feature map f_D and the top cell and noise feature f_{cell} and f_{noise} , obtaining similarity maps sim_{cell} and $\text{sim}_{\text{noise}}$. The computation are provided in Eq. 8 in the Appendix A (labeled as ϕ_4 and ϕ_5 in Fig. 2).

2.2.3. CONSENSUS-AWARE LOSS FUNCTION

During training, the model is guided to focus on regions where both the AI agent and lay annotators agree (CP and CN) while ignoring regions likely to contain noise. By combining the confidence map c and lay annotations y_l , CP and CN regions are highlighted, and sim_{cell} and $\text{sim}_{\text{noise}}$ further refine the focus on cell-like regions within DO and MC areas. The final supervised loss is defined in Eq. 2:

$$\begin{aligned} \omega_c &= \exp(c \cdot y_l + (1 - c) \cdot (1 - y_l)) & \omega_{\text{sim}} &= \exp(\text{sim}_{\text{cell}} - \text{sim}_{\text{noise}}) \\ \mathcal{L}_{\text{supervise}}(y_l, f(x; \theta)) &= (\mathcal{L}_{\text{Dice}} + \mathcal{L}_{\text{BCE}})(y_l, f(x; \theta)) \cdot \omega_c \cdot \omega_{\text{sim}} \end{aligned} \quad (2)$$

Where f is the segmentation model, θ are the trainable parameters, and $\mathcal{L}_{\text{Dice}}$ and \mathcal{L}_{BCE} are the Dice efficiency loss and Binary Cross-Entropy loss, respectively.

2.3. Contrastive Noise Separation

Using the final cell feature f_{cell} and noise feature f_{noise} , we aim to maximize their separation using a contrastive learning loss function in Eq. 3:

$$\mathcal{L}_{\text{contrastive}}(f_{\text{cell}}, f_{\text{noise}}) = (\mathcal{L}_{\text{KL}} + \mathcal{L}_{\text{MSE}})(\text{norm}(f_{\text{cell}}), \text{norm}(f_{\text{noise}})) \quad (3)$$

where \mathcal{L}_{KL} is the KL Divergence loss, and \mathcal{L}_{MSE} is the Mean Squared Error loss.

The final consensus-aware self-corrective learning loss combines $\mathcal{L}_{\text{supervise}}$ and $\mathcal{L}_{\text{contrastive}}$ to achieve robust training shown in Eq. 4:

$$\mathcal{L}_{\text{consensus-aware}}(y_l, f(x; \theta)) = \mathcal{L}_{\text{supervise}}(y_l, f(x; \theta)) + \mathcal{L}_{\text{contrastive}}(f_{\text{cell}}, f_{\text{noise}}) \quad (4)$$

3. Data and Experiment

3.1. Data

To evaluate the performance of the consensus-aware self-corrective learning framework, we collected a glomerular cell segmentation dataset. We utilized 21 whole slide images (WSIs) from normal adult cases in the nephrectomy dataset and HuBMAP. These slides were stained with Periodic Acid-Schiff (PAS), and were scanned at $20\times$ magnification. The WSIs were cropped into 512×512 -pixel segments to facilitate cell labeling. The cell labels are confined within glomeruli. The labeled cells included mesangial cells, endothelial cells, podocytes, and parietal epithelial cells. Labeling was performed in a partial-label manner, where each image contained a single class label with binary masks. The details of data collection are shown in Table 5 (In Appendix B).

Real Lay Annotation Dataset: Following the annotation process described in (Deng et al., 2023), two sets of annotations were obtained (1) directly from lay annotators and (2) underwent a quality assurance process conducted by experienced pathologists.

Reasoning-Generated Noise Datasets: To further explore the capabilities of the proposed method, we designed two reasoning-based noise generation pipelines to create FP and FN datasets:

- The FP data generation pipeline adds plausible noise labels by mimicking the size and characteristics of cells within nuclear regions near the ground truth labels in the glomeruli.
- The FN data generation pipeline randomly removes parts of the ground truth labels annotated by pathologists.

The visualizations of the three datasets are shown in Fig. 3, and the labeling accuracy for each dataset is presented in Table 1. The detailed pipelines are presented in Algorithm 1 and Algorithm 2 in the Appendix B.

Table 1: Label accuracy of each dataset. Dice similarity coefficient scores (%) are reported.

Dataset	Pod.	Mes.	Endo.	Pecs.	Mean
Real data	83.13	76.03	57.38	57.95	66.93
FP data	57.18	57.62	66.85	78.94	68.34
FN data	69.02	69.54	71.59	73.59	71.52

3.2. Experimental details

The dataset was split into training, validation, and testing sets in a 6:1:3 ratio at the WSI level, ensuring balanced distributions of injured and normal glomeruli across splits. All experiments used the same hyperparameter settings determined from an ablation study, employing the Adam optimizer (learning rate 0.0001, decay 0.99, epoch 100, loss weight 1:1) with augmentations such as affine transformations, contrast adjustments, and Gaussian noise. Model selection was based on the mean Dice score across the four cell classes in

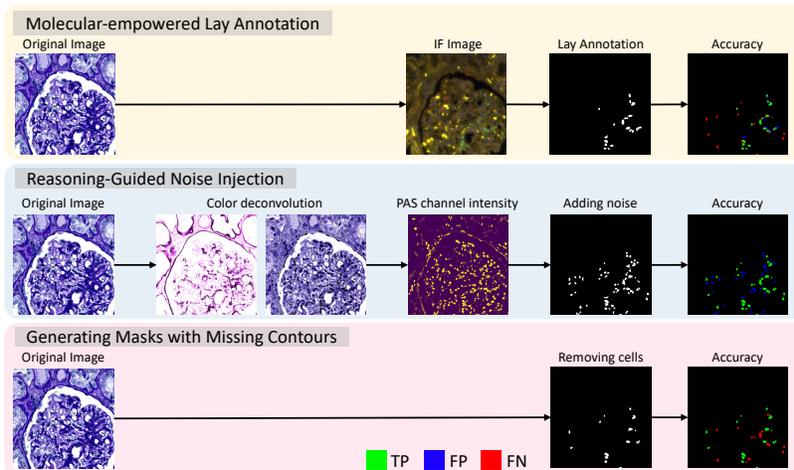


Figure 3: **Illustration of the Noisy Dataset.** The figure depicts one real lay annotation dataset and two noise generation pipelines used to create FP and FN datasets. The FP pipeline introduces plausible noise by simulating nuclear cell structures near glomerular regions, while the FN pipeline randomly removes annotated regions from the pathologist-provided ground truth labels. These processes are applied to evaluate the proposed method under challenging scenarios.

the validation set. All experiments were conducted on an NVIDIA RTX A6000 GPU for uniformity.

4. Results

4.1. Testing Set Segmentation Performance

We evaluate the proposed CASC-AI framework alongside other loss correction noisy label learning methods on three datasets. All methods were implemented with the same backbone and hyperparameters to ensure fair comparisons. The predictions are evaluated using Dice similarity coefficient scores on the testing datasets, where the labels have been corrected and verified by experienced pathologists.

Table 2 demonstrate that the proposed method achieves improvements compared to direct supervised learning and other baseline methods. This indicates that CASC-AI effectively leverages lay annotations while mitigating noise for enhanced segmentation performance.

Table 2: Performance of different noisy label learning methods. Dice similarity coefficient scores (%) are reported. The top 2 performed methods are marked as **red** and **blue**.

Method	Real Dataset					FP Dataset					FN Dataset				
	Pod.	Mes.	Endo.	Pecs.	Mean	Pod.	Mes.	Endo.	Pecs.	Mean	Pod.	Mes.	Endo.	Pecs.	Mean
Supervised	71.18	68.33	51.99	76.09	66.90	71.12	64.24	64.56	70.87	67.70	61.51	66.60	66.02	71.13	66.32
GCE (Zhang and Sabuncu, 2018)	66.94	51.25	49.71	55.56	55.86	62.71	62.27	66.16	66.96	64.52	56.17	49.86	49.71	49.91	51.41
NCE+NMAE (Ma et al., 2020)	49.92	49.86	49.71	49.91	49.85	49.92	49.86	49.71	49.91	49.85	49.92	49.86	49.71	49.91	49.85
NRDice (Wang et al., 2020)	71.00	52.75	49.72	65.62	59.77	71.00	52.75	49.72	65.62	59.77	52.48	49.86	52.85	49.91	51.28
CL (Deng et al., 2023)	74.00	67.26	69.53	73.89	71.17	65.24	65.89	69.04	73.78	68.49	71.92	67.40	70.94	73.05	70.83
CASC-AI (Ours)	74.93	68.88	72.24	75.94	73.00	68.49	66.24	70.64	74.75	70.03	72.85	70.04	72.63	74.90	72.60

4.2. Training Set Segmentation Performance

To evaluate the hypothesis that CASC-AI recognizes FP and FN during training, Table 3 presents Dice scores for TP predictions and Intersection over Union (IoU) scores for FP and

FN predictions. These results highlight that CASC-AI reduces predictions in FP regions while increasing predictions in FN regions, leading to corrections of the imperfect labels for accurate segmentation during the training phase.

Table 3: Performance on training dataset on TP, FP, and FN regions of the label. Dice similarity coefficient scores (%) are reported on TP, while IoU (%) are reported on FP and FN.

Method	Real Dataset			FP Dataset		FN Dataset	
	TP(Dice) \uparrow	FP(IoU) \downarrow	FN(IoU) \uparrow	TP(Dice) \uparrow	FP(IoU) \downarrow	TP(Dice) \uparrow	FN(IoU) \uparrow
Supervised	67.99	2.86	8.20	67.35	20.67	66.52	17.01
CASC-AI (Ours)	73.25	3.48	9.89	69.83	18.22	68.20	18.73

4.3. Ablation Study

We conducted an ablation study to identify the optimal hyperparameter settings for cell segmentation, using ground-truth labels corrected and verified by pathologists. Results shown in the Table 4 indicate that reducing the learning rate to 10^{-4} provides the best performance. Increasing the loss weights for the cell class during loss calculations and extending the training epochs did not lead to further performance gains.

Table 4: Performance on different hyperparameter settings. Dice similarity coefficient scores (%) are reported.

Max Epoch	Learning Rate	Loss Weights	Pod.	Mes.	Endo.	Pecs.	Mean
100	10^{-3}	1:1	73.65	68.99	70.06	73.73	71.61
100	10^{-3}	10:1	73.06	71.24	70.05	72.39	71.69
200	10^{-3}	1:1	74.22	70.33	69.88	74.93	72.34
100	10^{-4}	1:1	73.92	69.19	74.52	77.30	73.73
200	10^{-4}	1:1	75.01	67.79	74.33	76.70	73.46
100	10^{-5}	1:1	68.52	64.09	69.44	75.17	69.31

4.4. Limitations

This study has several limitations. We restricted the design to a **loss correction design**. Exploring additional paradigms of corrective learning (multi-network, co-training, etc.) could further enhance the performance of corrective learning. **Exploring additional backbones** represents a promising direction to better capture subtle patterns between cells and noise at the latent level, thus improving the overall cell segmentation performance and feature embedding quality. Furthermore, **analyzing noise distribution and patterns** within datasets as conditional information for model training could provide valuable insights and improve noise-label learning in future research.

5. Conclusion

In this work, we present the CASC-AI framework, a robust and consensus-aware self-corrective AI agent designed to address the challenges of cell segmentation in noisy datasets. By leveraging the Consensus Matrix to identify and prioritize agreement regions between human annotators and the AI agent, while adaptively weighting disagreement areas, the framework enhances segmentation reliability even in the presence of noisy annotations. This approach highlights the potential of incorporating an AI agent to correct human errors in the labels, while AI-driven corrective learning reduces reliance on expert labeling, paving the way for scalable and robust solutions in medical imaging and digital pathology.

Acknowledgments

This research was supported by NIH R01DK135597 (Huo), DoD HT9425-23-1-0003 (HCY), and KPMP Glue Grant. This work was also supported by Vanderbilt Seed Success Grant, Vanderbilt Discovery Grant, and VISE Seed Grant.

References

- Samuel P Border, John E Tomaszewski, Teruhiko Yoshida, Jeffrey B Kopp, Jeffrey B Hodgins, William L Clapp, Avi Z Rosenberg, Jill P Buyon, and Pinaki Sarder. Investigating quantitative histological characteristics in renal pathology using histolens. *Scientific reports*, 14(1):17528, 2024.
- Juan C Caicedo, Sam Cooper, Florian Heigwer, Scott Warchal, Peng Qiu, Csaba Molnar, Aliaksei S Vasilevich, Joseph D Barry, Harmanjit Singh Bansal, Oren Kraus, et al. Data-analysis strategies for image-based cell profiling. *Nature methods*, 14(9):849–863, 2017.
- Dorin Comaniciu and Peter Meer. Cell image segmentation for diagnostic pathology. *Advanced algorithmic approaches to medical image segmentation: State-of-the-art applications in cardiology, neurology, mammography and pathology*, pages 541–558, 2002.
- Ruining Deng, Yanwei Li, Peize Li, Jiacheng Wang, Lucas W Remedios, Saydolimkhon Agzamkhodjaev, Zuhayr Asad, Quan Liu, Can Cui, Yaohong Wang, et al. Democratizing pathological image segmentation with lay annotators via molecular-empowered learning. In *International Conference on Medical Image Computing and Computer-Assisted Intervention*, pages 497–507. Springer, 2023.
- Ruining Deng, Quan Liu, Can Cui, Tianyuan Yao, Juming Xiong, Shunxing Bao, Hao Li, Mengmeng Yin, Yu Wang, Shilin Zhao, et al. Hats: Hierarchical adaptive taxonomy segmentation for panoramic pathology image analysis. In *International Conference on Medical Image Computing and Computer-Assisted Intervention*, pages 155–166. Springer, 2024a.
- Ruining Deng, Quan Liu, Can Cui, Tianyuan Yao, Jialin Yue, Juming Xiong, Lining Yu, Yifei Wu, Mengmeng Yin, Yu Wang, et al. Prpseg: Universal proposition learning for panoramic renal pathology segmentation. In *Proceedings of the IEEE/CVF Conference on Computer Vision and Pattern Recognition*, pages 11736–11746, 2024b.
- Shujian Deng, Xin Zhang, Wen Yan, Eric I-Chao Chang, Yubo Fan, Maode Lai, and Yan Xu. Deep learning in digital pathology image analysis: a survey. *Frontiers of medicine*, 14:470–487, 2020.
- Noah F Greenwald, Geneva Miller, Erick Moen, Alex Kong, Adam Kagel, Thomas Dougherty, Christine Camacho Fullaway, Brianna J McIntosh, Ke Xuan Leow, Morgan Sarah Schwartz, et al. Whole-cell segmentation of tissue images with human-level performance using large-scale data annotation and deep learning. *Nature biotechnology*, 40(4):555–565, 2022.
- Junlin Guo, Siqi Lu, Can Cui, Ruining Deng, Tianyuan Yao, Zhewen Tao, Yizhe Lin, Marilyn Lions, Quan Liu, Juming Xiong, et al. How good are we? evaluating cell ai foundation models in kidney pathology with human-in-the-loop enrichment. *arXiv preprint arXiv:2411.00078*, 2024.

- Ruoyu Guo, Kunzi Xie, Maurice Pagnucco, and Yang Song. Sac-net: Learning with weak and noisy labels in histopathology image segmentation. *Medical Image Analysis*, 86: 102790, 2023.
- Bo Han, Quanming Yao, Xingrui Yu, Gang Niu, Miao Xu, Weihua Hu, Ivor Tsang, and Masashi Sugiyama. Co-teaching: Robust training of deep neural networks with extremely noisy labels. *Advances in neural information processing systems*, 31, 2018.
- Shih-Cheng Huang, Liyue Shen, Matthew P Lungren, and Serena Yeung. Gloria: A multimodal global-local representation learning framework for label-efficient medical image recognition. In *Proceedings of the IEEE/CVF International Conference on Computer Vision*, pages 3942–3951, 2021.
- John D Imig, Xueying Zhao, Ahmed A Elmarakby, and Tengis Pavlov. Interactions between podocytes, mesangial cells, and glomerular endothelial cells in glomerular diseases. *Frontiers in Physiology*, page 488, 2022.
- JoséA Jiménez-Heffernan, M Auxiliadora Bajo, Cristian Perna, Gloria del Peso, Juan R Larrubia, Carlos Gamallo, JoséA Sánchez-Tomero, Manuel López-Cabrera, and Rafael Selgas. Mast cell quantification in normal peritoneum and during peritoneal dialysis treatment. *Archives of pathology & laboratory medicine*, 130(8):1188–1192, 2006.
- Davood Karimi, Haoran Dou, Simon K Warfield, and Ali Gholipour. Deep learning with noisy labels: Exploring techniques and remedies in medical image analysis. *Medical image analysis*, 65:101759, 2020.
- Leeat Keren, Marc Bosse, Diana Marquez, Roshan Angoshtari, Samir Jain, Sushama Varma, Soo-Ryum Yang, Allison Kurian, David Van Valen, Robert West, et al. A structured tumor-immune microenvironment in triple negative breast cancer revealed by multiplexed ion beam imaging. *Cell*, 174(6):1373–1387, 2018.
- Geert Litjens, Thijs Kooi, Babak Ehteshami Bejnordi, Arnaud Arindra Adiyoso Setio, Francesco Ciompi, Mohsen Ghafoorian, Jeroen Awm Van Der Laak, Bram Van Ginneken, and Clara I Sánchez. A survey on deep learning in medical image analysis. *Medical image analysis*, 42:60–88, 2017.
- Liyun Lu, Mengxiao Yin, Liyao Fu, and Feng Yang. Uncertainty-aware pseudo-label and consistency for semi-supervised medical image segmentation. *Biomedical Signal Processing and Control*, 79:104203, 2023.
- Nicholas Lucarelli, Zoltan Laszik, Seth Winfree, Tarek M El-Achkar, Michael Eadon, Sanjay Jain, and Pinaki Sarder. Computational integration of codex and brightfield histology for cell annotation using deep learning. In *Medical Imaging 2024: Digital and Computational Pathology*, volume 12933, pages 347–350. SPIE, 2024.
- Xingjun Ma, Hanxun Huang, Yisen Wang, Simone Romano, Sarah Erfani, and James Bailey. Normalized loss functions for deep learning with noisy labels. In *International conference on machine learning*, pages 6543–6553. PMLR, 2020.
- Stéphane Olindo, Agnès Lézin, Philippe Cabre, Harold Merle, Martine Saint-Vil, Mireille Edimonana Kaptue, Aïssatou Signate, Raymond Césaire, and Didier Smadja.

- Htlv-1 proviral load in peripheral blood mononuclear cells quantified in 100 ham/tsp patients: a marker of disease progression. *Journal of the neurological sciences*, 237(1-2): 53–59, 2005.
- Maxime Oquab, Timothée Darcet, Théo Moutakanni, Huy Vo, Marc Szafraniec, Vasil Khalidov, Pierre Fernandez, Daniel Haziza, Francisco Massa, Alaaeldin El-Nouby, et al. Dinov2: Learning robust visual features without supervision. *arXiv preprint arXiv:2304.07193*, 2023.
- Aditya Pratapa, Michael Doron, and Juan C Caicedo. Image-based cell phenotyping with deep learning. *Current opinion in chemical biology*, 65:9–17, 2021.
- Șerban Vădineanu, Daniël Maria Pelt, Oleh Dzyubachyk, and Kees Joost Batenburg. An analysis of the impact of annotation errors on the accuracy of deep learning for cell segmentation. In *International Conference on Medical Imaging with Deep Learning*, pages 1251–1267. PMLR, 2022.
- Guotai Wang, Xinglong Liu, Chaoping Li, Zhiyong Xu, Jiugen Ruan, Haifeng Zhu, Tao Meng, Kang Li, Ning Huang, and Shaoting Zhang. A noise-robust framework for automatic segmentation of covid-19 pneumonia lesions from ct images. *IEEE Transactions on Medical Imaging*, 39(8):2653–2663, 2020.
- Dulharie T Wijeratne, Samitha Fernando, Laksiri Gomes, Chandima Jeewandara, Anushka Ginneliya, Supun Samarasekara, Ananda Wijewickrama, Clare S Hardman, Graham S Ogg, and Gathsaurie Neelika Malavige. Quantification of dengue virus specific t cell responses and correlation with viral load and clinical disease severity in acute dengue infection. *PLoS neglected tropical diseases*, 12(10):e0006540, 2018.
- Fuyong Xing and Lin Yang. Robust nucleus/cell detection and segmentation in digital pathology and microscopy images: a comprehensive review. *IEEE reviews in biomedical engineering*, 9:234–263, 2016.
- Tianwei Zhang, Lequan Yu, Na Hu, Su Lv, and Shi Gu. Robust medical image segmentation from non-expert annotations with tri-network. In *Medical Image Computing and Computer Assisted Intervention–MICCAI 2020: 23rd International Conference, Lima, Peru, October 4–8, 2020, Proceedings, Part IV 23*, pages 249–258. Springer, 2020.
- Zhilu Zhang and Mert Sabuncu. Generalized cross entropy loss for training deep neural networks with noisy labels. *Advances in neural information processing systems*, 31, 2018.
- Yi Zheng, Clarissa A Cassol, Saemi Jung, Divya Veerapaneni, Vipul C Chitalia, Kevin YM Ren, Shubha S Bellur, Peter Boor, Laura M Barisoni, Sushrut S Waikar, et al. Deep-learning-driven quantification of interstitial fibrosis in digitized kidney biopsies. *The American journal of pathology*, 191(8):1442–1453, 2021.

Appendix A. Formula of the Consensus-Aware Self-Corrective Learning

The cell features f_{cell} are distilled from the pixel-level feature map of the decoder’s last layer f_D , as shown in 5.

$$\begin{aligned}
 a_{\text{CP}} &= c \cdot y_l \\
 \text{Ind}_{\text{CP}} &= \text{argsort}(-a_{\text{CP}})[:k] \\
 f_{\text{cell}} &= \frac{1}{k} \sum_{i=1}^k f_D(\text{Ind}_{\text{CP}}[i])
 \end{aligned} \tag{5}$$

These regions, which potentially contain both real cells and noise, are self-recognized by the AI agent by incorporating confidence maps c and layer annotations y_l , as shown in 6:

$$\begin{aligned}
 a_{\text{DO}} &= c \cdot (1 - y_l) \\
 \text{Ind}_{\text{DO}} &= \text{argsort}(-a_{\text{DO}})[:k/2] \\
 a_{\text{MC}} &= (1 - c) \cdot y_l \\
 \text{Ind}_{\text{MC}} &= \text{argsort}(-a_{\text{MC}})[:k/2]
 \end{aligned} \tag{6}$$

The noise features f_{noise} are distilled from the features of noise regions (DO and MC) based on their similarity to the cell features f_{cell} , as defined in 7.

$$\begin{aligned}
 fm_{\text{noise}} &= f_D([\text{Ind}_{\text{DO}}, \text{Ind}_{\text{MC}}]) \\
 s_{\text{cell}} &= \frac{fm_{\text{noise}} \cdot f_{\text{cell}}}{\|fm_{\text{noise}}\| \|f_{\text{cell}}\|} \\
 w &= \text{softmax}(1 - \text{norm}(s_{\text{cell}})) \\
 f_{\text{noise}} &= w \cdot fm_{\text{noise}}
 \end{aligned} \tag{7}$$

The similarity between the feature map f_D and the top cell and noise features f_{cell} and f_{noise} is calculated to obtain similarity maps sim_{cell} and $\text{sim}_{\text{noise}}$, as defined in 8.

$$\begin{aligned}
 \text{sim}_{\text{cell}} &= \frac{f_D \cdot f_{\text{cell}}}{\|f_D\| \|f_{\text{cell}}\|} \\
 \text{sim}_{\text{noise}} &= \frac{f_D \cdot f_{\text{noise}}}{\|f_D\| \|f_{\text{noise}}\|}
 \end{aligned} \tag{8}$$

Appendix B. Data Collection and Experiments

B.1. Data Information

The details of the patch-level data collection are provided in Table 5.

Table 5: Summary of data collection for different cell classes.

Class Name	Abbreviation	Patch #	Size	Scale	Stain
Podocytes	Pod.	1147	512 ²	20×	PAS
Mesangial cells	Mes.	789	512 ²	20×	PAS
Glomerular endothelial cells	Endo.	715	512 ²	20×	PAS
Parietal epithelial cells	Pecs	2014	512 ²	20×	PAS

B.2. Reasoning-Generated Noise Pipeline

The detailed processes of Reasoning-Guided Noise Injection for FP data and Generating Masks with Missing Contours for FN data are illustrated in Algorithm 1 and Algorithm 2.

Algorithm 1: Reasoning-Guided Noise Injection (FP data)

Input: Pathological image X , Manual label Y , Intensity threshold T , Noise limit $limit$

Output: Processed image and noise mask

Load the pathological image X and corresponding manual label Y ;

Perform color deconvolution on X to compute stain-specific masks;

Select the PAS channel image and generate a binary mask M using intensity threshold T ;

Extract contours from M and sort them by proximity to existing annotations in Y ;

Determine the noise addition limit based on the number of cells in Y ;

foreach *new_contour* in sorted contours **do**

if *new_contour* overlaps with existing annotations or violates spatial constraints **then**

continue;

else

if *new_contour* size is outside the acceptable range for cells **then**

continue;

else

 Add *new_contour* to the final noise mask;

end

end

if number of added contours reaches *limit* **then**

break;

end

end

Save the processed image and the generated noise mask;

Algorithm 2: Generating Masks with Missing Contours (FN data)

Input: Image X , Binary mask M , Missing ratio `missing_ratio`

Output: Processed image and modified mask

Load the image X and the binary mask M ;

Extract contours from M ;

Shuffle the contours randomly;

Set `limit` $\leftarrow (1 - \text{missing_ratio}) \times \text{len}(\text{contours})$;

Initialize `new_mask` $\leftarrow 0$;

Initialize `cnt` $\leftarrow 0$;

foreach *contour* in *contours* **do**

 Draw contour on `new_mask`;

 Increment `cnt`;

if *cnt* reaches *limit* **then**

 | **break**;

end

end

Save the processed image and the generated noise mask;
